Time-optimal polarization transfer from an electron spin to a nuclear spin

Haidong Yuan,[1,*] Robert Zeier,[2,†] Nikolas Pomplun,[2,3,‡] Steffen J. Glaser,[2,§] and Navin Khaneja[4]
[1]*Department of Mechanical and Automation Engineering, The Chinese University of Hong Kong, Shatin, Hong Kong*
[2]*Department Chemie, Technische Universität München, Lichtenbergstrasse 4, 85747 Garching, Germany*
[3]*Bruker BioSpin GmbH, Silberstreifen 4, 76287 Rheinstetten, Germany*
[4]*Department of Electrical Engineering, IIT Bombay, Powai, Mumbai 400 076, India*
(Received 8 September 2015; published 9 November 2015)

Polarization transfers from an electron spin to a nuclear spin are essential for various physical tasks, such as dynamic nuclear polarization in nuclear magnetic resonance and quantum information processing on hybrid electron-nuclear spin systems. We present time-optimal schemes for electron-nuclear polarization transfers which improve on conventional approaches, and we thereby establish an important class of faster controls. We highlight how time-optimal polarization transfers and their optimality are related to the time optimality of unitary transformations. Moreover, our work develops generally applicable analytic methods for analyzing the limits in controlling quantum systems.

DOI: 10.1103/PhysRevA.92.053414 PACS number(s): 33.35.+r, 03.67.Ac, 33.25.+k, 02.30.Yy

I. INTRODUCTION

As the gyromagnetic ratio of an electron is two to three orders of magnitude larger than that of a nucleus, electron spins are much easier polarized than nuclear spins. This offers a way to improve the polarization of nuclear spins by transferring polarization from electron spins to nuclear spins; much higher nuclear spin polarization can be achieved as compared to a direct polarization. This idea has been widely used in various physical settings; for example, dynamic nuclear polarization (DNP) [1–6] employs this idea to dramatically improve the sensitivity of nuclear magnetic resonance (NMR) [7,8]. It is also frequently used on various hybrid electron-nuclear spin systems, such as organic single crystals [9], endohedral fullerenes [10–12], phosphorous donors in silicon crystals [13], and nitrogen-vacancy centers in diamond [14–17]. For example, in the case of nitrogen-vacancy centers in diamond, efficient polarization transfers are used to initialize the quantum state of nuclear spins for quantum information processing.

Efficient polarization transfers are practically achieved by properly engineered pulse sequences whose design is studied in the field of quantum control [18–23]. In recent years, significant progress has been made in quantum control for both numerical [24–37] and analytical [38–41] methods. Extensive knowledge has been gained on optimal pulse sequences for two- and three-level systems [42–56], two uncoupled spins [57,58], and two coupled spins [59–65]. Further advances have been made on how to optimally control multiple coupled spins [66–91]. These methods have been successfully applied in NMR [92,93] to designing broadband pulses [94–96] and decoupling sequences [97–102]. They have also been utilized in magnetic resonance imaging [25,103–105] and electron paramagnetic resonance [106].

In this context, our work contributes to the bottom-up approach in quantum information processing of analyzing, for example, the ultimate limits for controlling basic quantum systems. The knowledge obtained from these building blocks can be leveraged later in time-efficient control schemes applicable to medium-scale quantum information processing devices. Our contribution in this general context is threefold: By completely understanding the structure of time-optimal controls in this particular setting of an electron-nuclear spin system, we first identify ubiquitous features of general controlled quantum systems. Secondly, we provide a detailed analysis of how the time-optimal control of unitary transformations relates to that of state-to-state transformations (i.e., polarization transfers). Thirdly, we develop an arsenal of analytical tools for ascertaining and validating time-optimal controls.

In particular, we consider in this article time-optimal pulse sequences for polarization transfers from an electron spin to a nuclear spin. Relaxation and decoherence are in practice inevitable and result in a loss of signal. But their effect can be mitigated by short pulse sequences which allow for highly sensitive experiments. We analyze and explain how the form of time-optimal sequences depends on the direction of the polarization by studying time-optimal transfers for different directions.

Recent analytical [107] and numerical [108,109] studies focused on low-field single-crystal experiments, where the nuclear Larmor frequency and *pseudosecular* hyperfine interaction (see Sec. 3.5 of Ref. [1]) are comparable in magnitude. As in [110–113], we focus here on the cases of *secular* hyperfine coupling (see Sec. 3.5 of Ref. [1]). These assumptions are satisfied in liquid-state and high-field solid-state DNP.

We analyze two particular cases of polarization transfers and determine the corresponding time-optimal sequences. In Sec. II, we consider the transfer from the state S_z of the electron spin to the state I_z of the nuclear spin. The second time-optimal transfer from S_z to I_x is presented in Sec. III. And most interestingly, the corresponding optimal transfer time is reduced to 78.5% when compared to the transfer from S_z to I_z, which highlights that the transfer efficiency depends crucially on the target state of the nuclear spin. We discuss our results

*hdyuan@mae.cuhk.edu.hk
†robert.zeier@ch.tum.de
‡nikolas.pomplun@bruker.com
§steffen.glaser@tum.de

in Sec. IV, and the possibility of a nonsinusoidal carrier wave form is entertained in Sec. V. We conclude in Sec. VI, and certain details are relegated to Appendices A and B.

II. TRANSFER FROM S_z TO I_z

In this section, we study the polarization transfer from the initial state S_z to the final state I_z [114]. We assume a secular hyperfine coupling (see Sec. 3.5 of Ref. [1]). In the laboratory frame, the resulting Hamiltonian is given by

$$H = \omega_S S_z + \omega_I I_z + 2\pi A S_z I_z + 2\pi \tilde{u}_x(t) S_x + 2\pi \tilde{v}_x(t) I_x, \tag{1}$$

where ω_S and ω_I denote the respective Larmor frequencies of the electron and the nuclear spin, A represents the strength of the secular hyperfine coupling, and $\tilde{u}_x(t)$ and $\tilde{v}_x(t)$ are the amplitudes of the control fields. Here, $S_j = (\sigma_j \otimes \sigma_0)/2$ acts on the electron spin and $I_k = (\sigma_0 \otimes \sigma_k)/2$ acts on the nuclear spin with $j,k \in \{x,y,z\}$, where $\sigma_0 := \left(\begin{smallmatrix} 1 & 0 \\ 0 & 1 \end{smallmatrix}\right)$ denotes the identity matrix and the Pauli matrices are $\sigma_x := \left(\begin{smallmatrix} 0 & 1 \\ 1 & 0 \end{smallmatrix}\right)$, $\sigma_y := \left(\begin{smallmatrix} 0 & -i \\ i & 0 \end{smallmatrix}\right)$, and $\sigma_z := \left(\begin{smallmatrix} 1 & 0 \\ 0 & -1 \end{smallmatrix}\right)$. For typical NMR settings, only a single radio-frequency coil is used which can be assumed to be oriented along the x axis of the laboratory frame. Hence, only a single control $\tilde{v}_x(t)$ appears for the nuclear spin in the laboratory frame Hamiltonian of Eq. (1). We assume in this work that the carrier wave form for the nuclear spin has a sinusoidal shape, i.e., $\tilde{v}_x(t) = v(t)\cos[\omega_I^{\mathrm{rf}} t + \phi(t)]$ with amplitude $v(t) \leqslant 2v_{\max}$ and phase ϕ_0. Here, ω_I^{rf} is the carrier frequency of the radio-frequency irradiation and $2v_{\max}$ denotes the maximal control amplitude (in the laboratory frame). This choice of $\tilde{v}_x(t)$ is motivated by the properties (e.g., bandwidth limitations) of the usually available wave form generators and amplifiers. More general carrier wave forms are discussed in Sec. V.

By switching to the rotating frame of $\omega_S S_z + \omega_I^{\mathrm{rf}} I_z$ corresponding to the carrier frequencies ω_S and $\omega_I^{\mathrm{rf}} = \omega_I - \omega_I^{\mathrm{off}}$ and applying the rotating wave approximation, we get an effective Hamiltonian

$$\begin{aligned} H_{\mathrm{rot}} &= +\omega_I^{\mathrm{off}} I_z + 2\pi A S_z I_z \\ &\quad + H_{\mathrm{rot}}^{\mathrm{mw}} + H_{\mathrm{rot}}^{\mathrm{rf}}, \quad \text{where} \\ H_{\mathrm{rot}}^{\mathrm{mw}} &:= 2\pi u_x(t) S_x + 2\pi u_y(t) S_y, \\ H_{\mathrm{rot}}^{\mathrm{rf}} &:= 2\pi v_x(t) I_x + 2\pi v_y(t) I_y. \end{aligned} \tag{2}$$

One can obtain any desired offset term $\omega_I^{\mathrm{off}} I_z$ in the drift term of H_{rot} in Eq. (2) by suitably choosing the carrier frequency ω_I^{rf} [115]. For simplicity, ω_I^{off} is set to zero in the following. The microwave-frequency control pulses on the electron spin and the radio-frequency control pulses on the nuclear spin are given by $H_{\mathrm{rot}}^{\mathrm{mw}}$ and $H_{\mathrm{rot}}^{\mathrm{rf}}$, respectively. The control amplitudes $u_x(t)$, $u_y(t)$, $v_x(t)$, and $v_y(t)$ satisfy the bounds

$$\sqrt{u_x^2(t) + u_y^2(t)} \leqslant u_{\max} \quad \text{and} \quad \sqrt{v_x^2(t) + v_y^2(t)} \leqslant v_{\max},$$

where $u_{\max}$ and $v_{\max}$ denote the maximal available amplitudes of the control fields in the rotating frame for a given experiment. This is a result of the rotating wave approximation, which reduces the maximal control amplitude of $2v_{\max}$ in laboratory frame to $v_{\max}$ in the rotating frame [8]. In the following, we will assume that $u_{\max} \gg A \gg v_{\max}$ and neglect the time needed to apply operations that can be generated by the hyperfine coupling and the controls on the electron spin [116].

Time-optimal transformations are essentially only limited by the weak controls on the nuclear spin. The optimal strategy to achieve a desired transfer can be inferred from the structure of cosets with respect to the fast operations [59,66,110]. Here, the fast operations are given by the hyperfine coupling and the strong controls on the electron spin. The transformation U which transfers S_z to $I_z = U S_z U^{-1}$ will be suitably decomposed into a product $U = U_2 U_1$. The unitary U_1 transfers the initial state S_z to the intermediate state $2S_z I_z = U_1 S_z U_1^{-1}$, and it can be generated using only fast operations. In addition, the unitary U_2 transfers the intermediate state $2S_z I_z$ to the final state $I_z = U_2(2S_z I_z)U_2^{-1}$, and one has to use the weak controls on the nuclear spin in order to generate U_2. Below, we will provide a time-optimal scheme to produce U_2. This also results in a time-optimal scheme for U as any faster scheme for U would also imply a faster one for $U_2 = U U_1^{-1}$.

The polarization transfer from S_z to I_z can be decomposed into the following steps [117]:

$$S_z \xrightarrow{(\pi/2)S_y} S_x \xrightarrow{\pi S_z I_z} 2S_y I_z \xrightarrow{(\pi/2)S_x} 2S_z I_z \xrightarrow{\pi S^\beta I_y} I_z, \tag{3}$$

where we denote

$$S^\alpha := \begin{pmatrix} 1 & 0 \\ 0 & 0 \end{pmatrix} \otimes \sigma_0 \quad \text{and} \quad S^\beta := \begin{pmatrix} 0 & 0 \\ 0 & 1 \end{pmatrix} \otimes \sigma_0,$$

then $\pi S^\beta I_y = -\pi S_z I_y + \pi I_y/2$. As shown in Eq. (3), the polarization transfer from S_z to $2S_z I_z$ is accomplished using an INEPT-type transfer [8,118]: First, we apply a hard $\pi/2$ pulse to the electron spin along the $+y$ direction (i.e., S_y). Then, we let the hyperfine coupling evolve for the duration of $1/(2A)$ units of time. Another hard $\pi/2$ pulse on the electron spin along the $+x$ direction completes the transfer to $2S_z I_z$. All of these steps take negligible time, since they are either local operations on the electron spin or operations which can be generated by the coupling. In conclusion, we can completely focus on the last step in Eq. (3) where we need to generate the propagator

$$U_y^\beta(\theta) = \exp(-i\theta S^\beta I_y) = \exp\left[-i\left(-\theta S_z I_y + \frac{\theta}{2} I_y\right)\right] \tag{4}$$

for $\theta = \pi$. The operator in the exponent of $U_y^\beta(\theta)$ in Eq. (4) is a single-transition operator [1,8]. In particular, the operator $U_y^\beta(\pi) = \exp(-i\pi S^\beta I_y)$ describes a transition-selective π rotation around the y axis in the subspace spanned by the basis states $|\beta\alpha\rangle$ and $|\beta\beta\rangle$, where the subspace corresponds to the β component of the nuclear spin doublet at frequency $\omega_I/(2\pi) + A/2$ [119] as shown in Figs. 1 and 2. Here, $|\alpha\rangle$ and $|\beta\rangle$ are eigenstates of S_z and I_z, e.g., $S_z|\alpha\rangle = |\alpha\rangle/2$ and $S_z|\beta\rangle = -|\beta\rangle/2$.

In the following, we determine a time-optimal scheme to produce the unitary $U_y^\beta(\pi)$. The set of all unitaries which transfer $2S_z I_z$ to I_z are discussed in Appendix A 1, where we also show by extending the results in the current section that choosing a different element from this set of unitaries does not lead to a shorter transfer time.

To determine the optimal transfer, we switch to the interacting frame of $2\pi A S_z I_z$ by applying the transformation

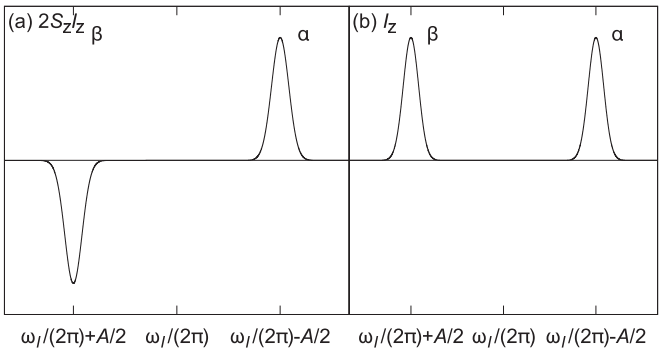

FIG. 1. Schematic depiction of the absorption profiles for (a) $2S_zI_z$ and (b) I_z.

$\exp(i2\pi A S_z I_z t) H_{\rm rot} \exp(-i2\pi A S_z I_z t)$. The Hamiltonian of Eq. (2) changes to [120]

$$\begin{aligned} H_{\rm int} = &+ 2\pi u_x(t)[\cos(\pi At)S_x - \sin(\pi At)2S_yI_z] \\ &+ 2\pi u_y(t)[\cos(\pi At)S_y + \sin(\pi At)2S_xI_z] \\ &+ 2\pi v_x(t)[\cos(\pi At)I_x - \sin(\pi At)2S_zI_y] \\ &+ 2\pi v_y(t)[\cos(\pi At)I_y + \sin(\pi At)2S_zI_x] \end{aligned} \quad (5)$$

which can be also written as

$$\begin{aligned} H_{\rm int} = &+ 2\pi u_x(t)[\cos(\pi At)S_x - \sin(\pi At)2S_yI_z] \\ &+ 2\pi u_y(t)[\cos(\pi At)S_y + \sin(\pi At)2S_xI_z] \\ &+ 2\pi [v_x(t)\cos(\pi At)I_x + v_y(t)\sin(\pi At)2S_xI_x] \\ &- 2\pi [v_x(t)\sin(\pi At) - v_y(t)\cos(\pi At)]S^\alpha I_y \\ &+ 2\pi [v_x(t)\sin(\pi At) + v_y(t)\cos(\pi At)]S^\beta I_y, \end{aligned} \quad (6)$$

where $S^\alpha I_y = S_zI_y + I_y/2$ and $S^\beta I_y = -S_zI_y + I_y/2$.

We aim at generating the operator $U_y^\beta(\pi)$ in minimum time, which corresponds to maximizing the coefficient $2\pi[v_x(t)\sin(\pi At) + v_y(t)\cos(\pi At)]$ in front of $S^\beta I_y$. The Cauchy-Schwarz inequality implies

$$\begin{aligned} &[v_x(t)\sin(\pi At) + v_y(t)\cos(\pi At)]^2 \\ &\leqslant \left[v_x^2(t) + v_y^2(t)\right][\sin^2(\pi At) + \cos^2(\pi At)] \leqslant v_{\rm max}^2, \end{aligned}$$

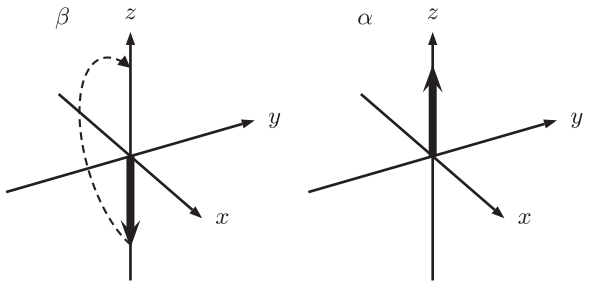

FIG. 2. In the polarization transfer from $2S_zI_z$ to I_z, the β component of the nuclear spin doublet is rotated by an angle of π around the y axis and the α component is left invariant (both visualized in the interaction frame). Note that the electron spin is in the state $|\beta\rangle$ on the left-hand side and in the state $|\alpha\rangle$ on the right-hand side.

where the second inequality is a consequence of the constraints on the amplitude of the control fields. The maximal value of $2\pi[v_x(t)\sin(\pi At) + v_y(t)\cos(\pi At)]$ is denoted by $2\pi v_{\rm max}$ and it can be achieved by choosing the controls

$$u_x(t) = u_y(t) = 0, \quad (7a)$$

$$v_x(t) = v_{\rm max}\sin(\pi At), \quad v_y(t) = v_{\rm max}\cos(\pi At). \quad (7b)$$

To understand that this choice generates the desired operator, one can substitute the controls in the Hamiltonian with the chosen values and obtains

$$\begin{aligned} H_{\rm int} = &+ 2\pi v_{\rm max}\sin(\pi At)\cos(\pi At)I_x \\ &+ 2\pi v_{\rm max}\cos(\pi At)\sin(\pi At)2S_zI_x \\ &+ 2\pi v_{\rm max}\cos(2\pi At)S^\alpha I_y + 2\pi v_{\rm max}S^\beta I_y. \end{aligned}$$

Since $A \gg v_{\rm max}$, average Hamiltonian theory implies that the first three terms average out to zero; and one is left with the desired Hamiltonian $2\pi v_{\rm max}S^\beta I_y$.

The minimum time to generate $U_y^\beta(\pi)$ is then fixed by the relation $2\pi v_{\rm max}T_{\rm min} = \pi$, and one obtains

$$T_{\rm min} = 1/(2v_{\rm max}).$$

The presented time-optimal control corresponds to a radio-frequency irradiation at frequency $\omega_I/(2\pi) + A/2$ with duration $T_{\rm min}$, which results in a transition-selective inversion of the β line of the nuclear spin doublet. This belongs to the class of controls presented in Ref. [110] and is also closely related to selective population inversion (SPI) experiments [121–124].

We can also compute the maximal transfer efficiency $\eta_{\rm max}(T)$ for a given time T. The operator $U_y^\beta(\theta)$ transfers the state $2S_zI_z$ to the state

$$\begin{aligned} U_y^\beta(\theta)(2S_zI_z)\left[U_y^\beta(\theta)\right]^\dagger = &\cos^2\left(\tfrac{\theta}{2}\right)2S_zI_z + \cos\left(\tfrac{\theta}{2}\right)\sin\left(\tfrac{\theta}{2}\right)2S_zI_x \\ &- \cos\left(\tfrac{\theta}{2}\right)\sin\left(\tfrac{\theta}{2}\right)I_x + \sin^2\left(\tfrac{\theta}{2}\right)I_z. \end{aligned} \quad (8)$$

For $\theta = 2\pi v_{\rm max}T$, we get the maximal transfer efficiency

$$\eta_{\rm max}(T) = \sin^2\left(\tfrac{\theta}{2}\right) = \sin^2(\pi v_{\rm max}T) \quad (9)$$

for the transfer to I_z. Note that $\eta_{\rm max}(T_{\rm min}) = 1$.

We compare our analytic results with numerical optimizations for achieving the transfer from S_z to I_z as shown in Fig. 3 (cf. [111–113]). For these optimizations, the hyperfine coupling constant is chosen as $A = 10$ MHz and the maximal allowed radiation amplitudes are set to $u_{\rm max} = 1$ MHz and $v_{\rm max} = 20$ kHz [125]. In Fig. 3, the transfer is completed after $25\ \mu{\rm s} = 1/(2v_{\rm max})$ units of time which agrees with the analytically computed time. Moreover, the form of the numerically optimized controls compares nicely with the analytic results: the values of $u_x(t)$ and $u_y(t)$ are most of the time small (except for the beginning), and $v_x(t)$ and $v_y(t)$ have a sinusoidal form with the maximal allowed amplitude.

III. TRANSFER FROM S_z TO I_x OR I_y

We analyze now how to time-optimally transfer polarization from the state S_z to I_x (and similarly for the transfer to I_y).

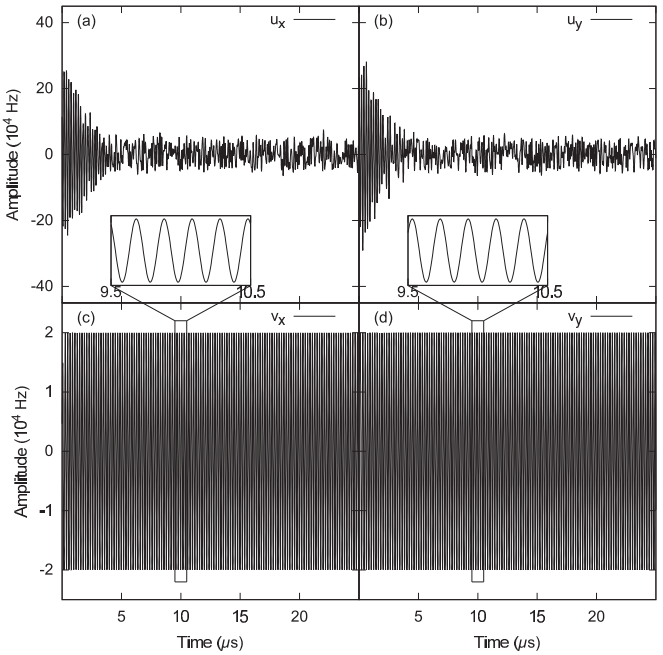

FIG. 3. Numerically optimized pulses for the polarization transfer from S_z to I_z. The coupling strength is 10 MHz and the bounds on the microwave and radio-frequency amplitudes are $u_{\max} = 1$ MHz and $v_{\max} = 20$ kHz, respectively. The maximal transfer efficiency is reached after 25 μs. The insets show magnified parts of the controls $v_x(t)$ and $v_y(t)$ in order to illustrate their form.

The considered transfer consists of the following steps:

$$S_z \xrightarrow{(\pi/2)S_y} S_x \xrightarrow{\pi S_z I_z} 2S_y I_z \xrightarrow{(\pi/2)S_x} 2S_z I_z \xrightarrow{(\pi/2)S^\alpha I_y - (\pi/2)S^\beta I_y} I_x, \tag{10}$$

where $\frac{\pi}{2} S^\alpha I_y - \frac{\pi}{2} S^\beta I_y = \pi S_z I_y$. As in Sec. II, we can focus on generating the final propagator $\tilde{U}_2 = \exp(-i\pi S_z I_y)$ in the product $\tilde{U} = \tilde{U}_2 U_1$. The transfer $I_x = \tilde{U} S_z \tilde{U}^{-1}$ is decomposed into a fast transfer to the intermediate state $2S_z I_z = U_1 S_z U_1^{-1}$ and a slow transfer to final state $I_x = \tilde{U}_2(2S_z I_z)\tilde{U}_2^{-1}$. Building on the results in this section, we prove in Appendix A 2 that one cannot reduce the transfer time by substituting $\tilde{U}_2$ with a different unitary V satisfying $I_x = V(2S_z I_z)V^{-1}$.

Previously, the propagator $\exp(-i\pi S_z I_y)$ in the final step has been achieved [110] by applying a transition-selective radio-frequency $-\pi/2$ pulse along the y direction at the β transition with frequency $\omega_I/(2\pi) + A/2$ as well as a transition-selective radio-frequency $\pi/2$ pulse along the y direction at the α transition with frequency $\omega_I/(2\pi) - A/2$ (see Fig. 4). In the rotating frame of Eq. (2), this irradiation scheme on the nuclear spin corresponds to a radio-frequency Hamiltonian of the form

$$\begin{aligned} H_{\text{rot}}^{\text{rf}} =& -2\pi \frac{v_{\max}}{2} \cos(\pi A t) I_x - 2\pi \frac{v_{\max}}{2} \sin(\pi A t) I_y \\ &+ 2\pi \frac{v_{\max}}{2} \cos(-\pi A t) I_x + 2\pi \frac{v_{\max}}{2} \sin(-\pi A t) I_y \\ =& -2\pi v_{\max} \sin(\pi A t) I_y. \end{aligned}$$

Note that in this scheme the α and β transitions can only be irradiated with a radio-frequency amplitude of $v_{\max}/2$ in order not to exceed the maximal available radio-frequency amplitude $v_{\max}$ for the overall irradiation at the nuclear spin. Hence, the duration for the simultaneous $\pm\pi/2$ pulses along the y direction at the α and β transitions is equal to $1/(2v_{\max})$. This conventional transfer is optimal if one considers *only* pulses at the frequencies $\omega_I/(2\pi) \pm A/2$ of the nuclear-spin doublet (refer to [110] and the discussion in Sec. IV).

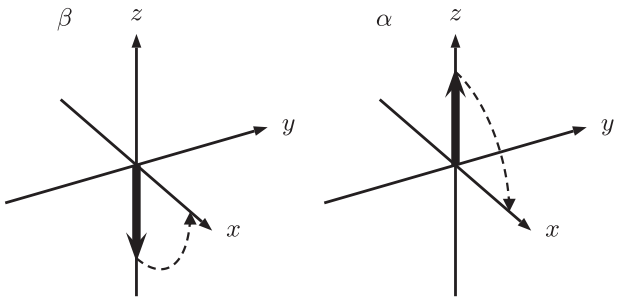

FIG. 4. In the polarization transfer from $2S_z I_z$ to I_x the β component of the nuclear spin doublet is rotated by $-\pi/2$ around the y axis and the α component is rotated by $\pi/2$ around the y axis (both visualized in the interaction frame).

Here, we show that shorter pulses are possible if one considers more general irradiation schemes. Without exceeding $v_{\max}$, shorter pulses can be obtained by irradiating at the frequencies $\omega_I/(2\pi) \pm A/2$ with higher intensity since the resulting higher amplitude can be then decreased by irradiating at *additional* well selected frequencies. Our approach is quite effective although it might seem counterintuitive at first.

In the interaction frame of $2\pi A S_z I_z$, the Hamiltonian is again given by Eq. (5). In order to generate the operator $\exp(-i\pi S_z I_y)$ in minimum time, we maximize the coefficient $-2\pi v_x(t)\sin(\pi A t)$ of $2S_z I_y$. Note that

$$\begin{aligned} -2\pi v_x(t)\sin(\pi A t) &\leqslant |-2\pi v_x(t)\sin(\pi A t)| \\ &\leqslant 2\pi v_{\max} |\sin(\pi A t)|, \end{aligned}$$

where the second equality is implied by the constraint $|v_x(t)| \leqslant \sqrt{v_x^2(t) + v_y^2(t)} \leqslant v_{\max}$ on the control amplitudes. Therefore, the maximal value $2\pi v_{\max}|\sin(\pi A t)|$ for $-2\pi v_x(t)\sin(\pi A t)$ can be attained by choosing the controls

$$u_x(t) = u_y(t) = v_y(t) = 0, \tag{11a}$$

$$v_x(t) = -\text{sgn}[\sin(\pi A t)] v_{\max}. \tag{11b}$$

This means that $v_x(t)$ is a square wave such that $v_x(t) = v_{\max}$ when $\sin(\pi A t) < 0$ and $v_x(t) = -v_{\max}$ when $\sin(\pi A t) > 0$. Inserting the controls of Eq. (11) into Eq. (6) results in the average Hamiltonian

$$\bar{H}_{\text{int}} = 4 v_{\max}(S^\alpha I_y - S^\beta I_y). \tag{12}$$

Creating the required $\pm\pi/2$ rotations shown in Fig. 4 results in the condition $4 v_{\max} T_{\min} = \pi/2$ and we obtain the minimum time

$$T_{\min} = \pi/(8 v_{\max})$$

for generating $\exp(-i\pi S_z I_y)$ in the interaction frame. The duration of the transfer is reduced to 78.5% of the length of the conventional pulse sequence. By transforming the operator back to the rotating frame, we obtain the op-

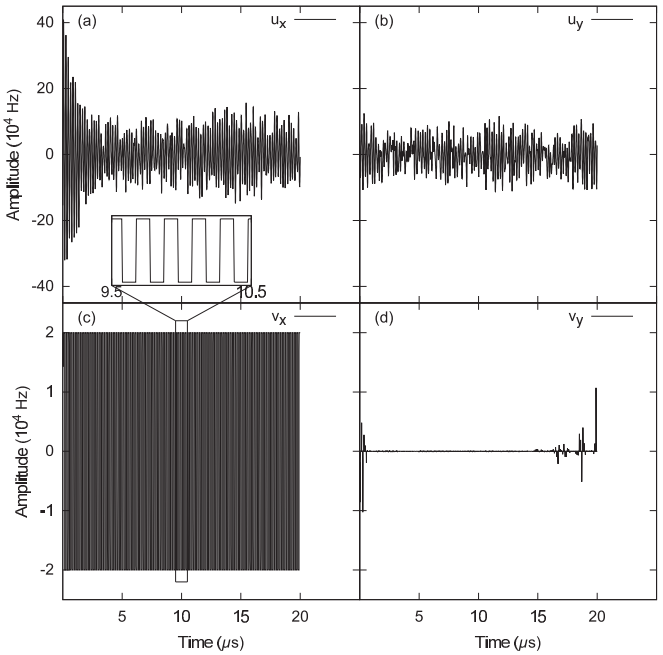

FIG. 5. Numerically optimized pulses for the polarization transfer from S_z to I_x. The coupling strength is 10 MHz and the bounds on the microwave and radio-frequency amplitudes are given by $u_{\max} = 1$ MHz and $v_{\max} = 20$ kHz, respectively. The maximal transfer efficiency is reached after 20 μs. The inset shows a magnified part of the control $v_x(t)$ in order to illustrate its form.

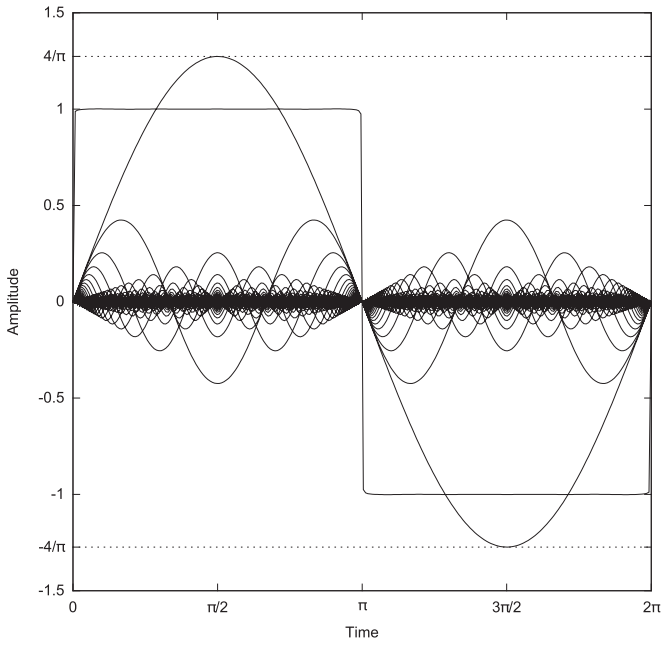

FIG. 6. Decomposition of a square wave into sine waves: a large number of harmonics sum to an approximate square wave. The first harmonic has an amplitude of $4/\pi$, while the square wave has an amplitude of 1. Note that the amplitude and time in this figure are considered as unitless.

erator $\exp(-i\phi S_z I_z)\exp(-i\pi S_z I_y)\exp(i\phi S_z I_z)$ where $\phi = 2\pi A T_{\min}$ denotes the phase accumulated during the time $T_{\min} = \pi/(8v_{\max})$. The effect of this superfluous phase ϕ can be reversed using the hyperfine coupling $2\pi A S_z I_z$ which takes only a negligible time period as the coupling strength A is much larger than the control strength $v_{\max}$ of the nuclear spin. Thus, the minimum time in the rotating frame is also given by $\pi/(8v_{\max})$. Similarly as in Eq. (8), we compute the maximal transfer efficiency

$$\eta_{\max}(T) = \sin(4v_{\max}T) \tag{13}$$

that can be reached for the polarization transfer from S_z to I_x in a specified time T.

Transferring the state from S_z to I_y is similar. We set $u_x(t) = u_y(t) = v_x(t) = 0$ and maximize the coefficient $-2\pi v_y(t)\sin(\pi At)$ of $-2S_z I_x$ in Eq. (5) by setting $v_y(t) = -\mathrm{sgn}[\sin(\pi At)]v_{\max}$. The minimum time for this case is also given by $\pi/(8v_{\max})$.

A numerically optimized pulse sequence for transferring polarization from S_z to I_x is shown in Fig. 5 (cf. [111–113]). The maximal transfer efficiency is reached after 20 μs, which is consistent with the analytical result of $\pi/(8v_{\max}) \approx 19.635$ μs.

IV. DISCUSSION

A. Explaining the speedup in Sec. III

We see that the minimum time for transferring S_z to I_x or I_y is shorter by a factor of $\pi/4 \approx 78.5\%$ when compared to the minimum time for transferring S_z to I_z. This factor can be explained by a closer examination of the pulse sequences. The radio-frequency sequence for the transfer from S_z to I_z shows a sine-cosine wave modulation of maximal amplitude for the v_x and v_y components (see Fig. 3). However, the radio-frequency sequence for the transfer from S_z to I_x consists of a square wave of maximal amplitude for the v_x component of the control (see Fig. 5). The higher effective amplitude at the two frequencies $\omega_I/(2\pi) \pm A/2$ and the shorter transfer time can be explained by decomposing the square wave into a sum of sine waves:

$$f_{\text{square}}(t) = \mathrm{sgn}[\sin(\pi At)] = \frac{4}{\pi}\sum_{n\ \text{odd},\, n\geqslant 1}\frac{1}{n}\sin(nAt).$$

This is illustrated in Fig. 6 where the first sine wave function has an amplitude which is larger by a factor of $4/\pi$ when compared to the amplitude of the square wave. Therefore, the square wave contains implicitly a sine wave with a higher effective amplitude. This implies that the duration of the simultaneous $\pm\pi/2$ rotations of the α and β components of the nuclear spin doublet (see Fig. 4) is shorter by a factor of $\pi/4$.

The square-modulated transfer sequence is optimal but needs infinite bandwidth. We also studied numerically how the maximal transfer efficiency varies as a function of time and bandwidth limitations. The results are shown in Fig. 7 (cf. [111–113]). In the case of infinite bandwidth, the results are consistent with the analytical results. The transfer functions $\sin^2(\pi v_{\max}t)$ and $\sin(4v_{\max}t)$ for the respective transfers from S_z to I_z and I_x have been obtained in Eqs. (9) and (13).

We compare our results to the time-optimal synthesis of unitary transformations in [110]. Motivated by energy considerations, only irradiations at the two resonance frequencies $\omega_I/(2\pi) \pm A/2$ of the control system were considered in [110]. This did not allow for the faster scheme obtained in

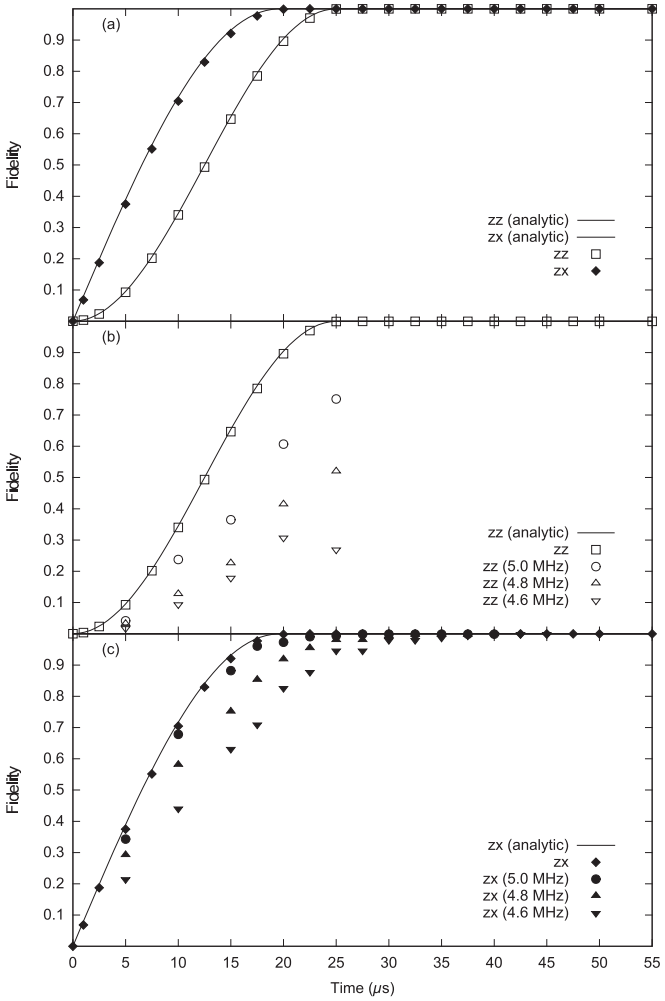

FIG. 7. The maximal transfer efficiency (i.e., fidelity) is shown for the transfers from S_z to I_z and I_x in (a). The coupling strength is 10 MHz, and the control strengths are $u_{\max} = 20$ kHz and $v_{\max} = 1$ MHz. In (b), data points for the transfer from S_z to I_z are also shown for the bandwidth-limited cases with bounds of 5.0, 4.8, and 4.6 MHz. Similarly, data points for the transfer from S_z to I_x are shown in (c).

Sec. III which has been also observed numerically in [111–113]. The numerical results in Fig. 7 also show that the faster scheme of Sec. III is—in a strict sense—only applicable in the case of infinite bandwidth. It provides, in general, superior results, but its benefit depends on the available bandwidth.

The irradiations at the different frequencies can be clearly observed in Fig. 8 where the normalized amplitudes of the short-time Fourier transform [126] are plotted for the relevant cases (using the method and implementation of [127]). The important difference between the controls of Fig. 3 for the polarization transfer from S_z to I_z and the controls of Fig. 5 for the transfer from S_z to I_x manifest itself in the short-time Fourier transforms of the v parts of the controls which are visible in Figs. 8(c) and 8(d). In Fig. 8(c), one notices the characteristic frequency of $A/2 = 5$ MHz. In contrast to Fig. 8(c), many more frequencies appear in Fig. 8(d) at multiples of the frequencies $\pm A/2$. This agrees with the square-wave form of the control v_x in Fig. 5.

In a general context, our results can also be interpreted as a connection between energy and time optimizations for given bounds on the control amplitudes. The energy optimization leads to a sinusoidal solution, while the time optimization leads to a square wave (see Fig. 5). This phenomenon has been also observed for the simultaneous inversion of two uncoupled spins [57,58] where a minimum energy solution was related to the first harmonic in the Fourier expansion of the time-optimal solution. The same reasoning applies here to the solutions of Sec. III.

B. Physical intuition for the time-optimal polarization transfers of Secs. II and III

We discuss now how the time-optimal polarization transfers obtained in Secs. II and III can be understood from a physical point of view. Recall that we decompose the transfer from S_z to I_z in Sec. II into a sequence of partial transfer step as given in Eq. (3). As discussed in Sec. II, the last step

$$2S_zI_z \xrightarrow{\pi S^\beta I_y} I_z \tag{14}$$

from $2S_zI_z$ to I_z is the critical one for determining the time-optimal control scheme. The unitary $U_y^\beta(\pi) = \exp(-i\pi S^\beta I_y)$ from Eq. (4) transfers $2S_zI_z$ to I_z, and the choice of this unitary is readily inferred from Fig. 2. This corresponds to the physical intuition of only flipping the β component by π to realize the transfer from spin alignment to spin polarization as in the classical SPI experiment [121–124]. Although the explicit form of the time-optimal controls in Eq. (7) (see also Fig. 3) implementing the unitary $U_y^\beta(\pi)$ could have been anticipated from physical intuition, the detailed mathematical derivation of Sec. II puts this on a sound foundation. Additional arguments are required for completing the argument: all unitaries which can achieve the polarization transfer in Eq. (14) are obtained in Appendix A 1, and it is then verified that these unitaries do not lead to faster control schemes. Therefore, our mathematical analysis explains how and under which conditions the physical intuition matches with the time-optimal solution.

A similar reasoning applies to the transfer form S_z to I_x, which is analyzed in Sec. III and where the last step in the transfer sequence of Eq. (10) is given by

$$2S_zI_z \xrightarrow{(\pi/2)S^\alpha I_y-(\pi/2)S^\beta I_y} I_x. \tag{15}$$

The corresponding unitary propagator $\exp(-i\pi S_zI_y) = \exp[-i(\frac{\pi}{2}S^\alpha I_y - \frac{\pi}{2}S^\beta I_y)]$ again agrees with the physical intuition to flip the α and β components by $\pi/2$ around the y and $-y$ axis, respectively, as illustrated in Fig. 4. The time-optimal implementation for this propagator is given in Eq. (11) (see also Fig. 5). Here, the optimal control scheme differs significantly from the intuitive approach, which would correspond to simultaneously irradiate transition-selective pulses at the frequencies $\omega_I/(2\pi) \pm A/2$, and identifies a more general class of controls than previously considered [110] (see Sec. IV A). The analysis is completed in Appendix A 2 by verifying that all other unitaries achieving the transfer of Eq. (15) cannot be implemented in a shorter time. In summary, our results match well with physical insight but go well beyond what can be grasped directly.

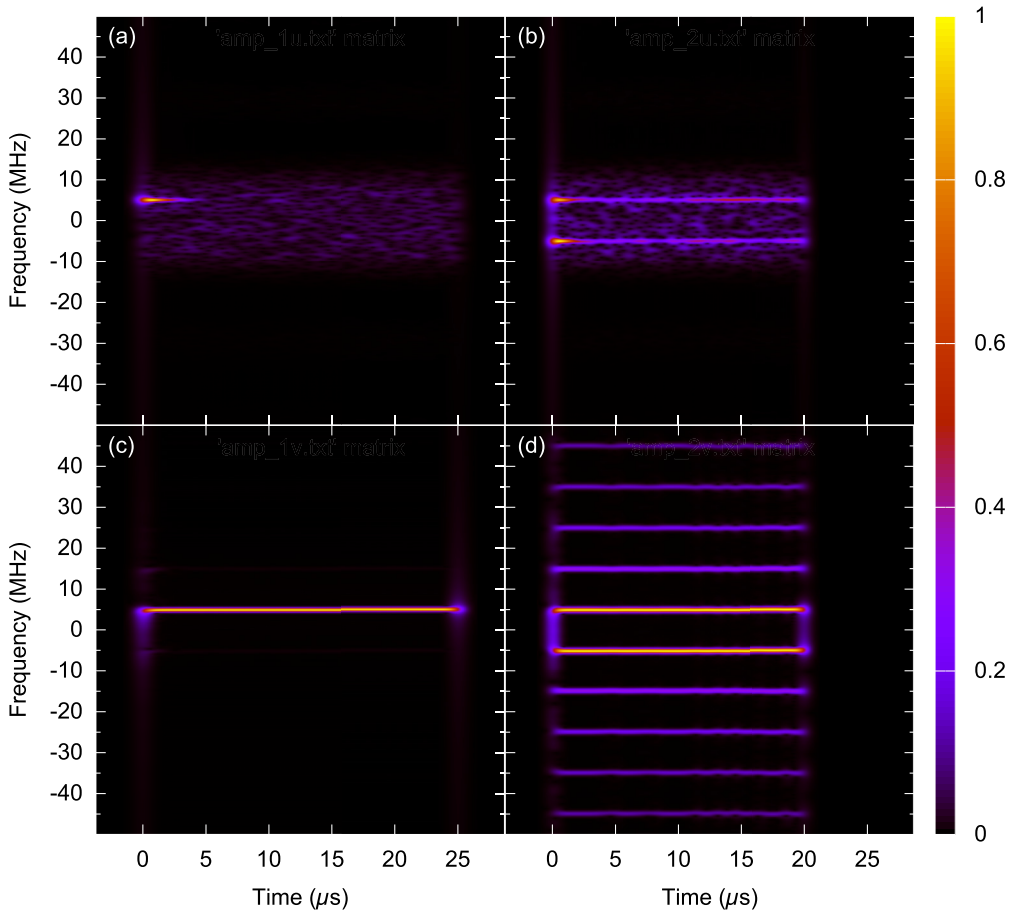

FIG. 8. (Color online) Normalized amplitudes of the short-time Fourier transform for different controls: (a) u controls of Fig. 3, (b) u controls of Fig. 5, (c) v controls of Fig. 3, and (d) v controls of Fig. 5. In (c), (essentially) only the characteristic frequency of $A/2 = 5$ MHz is present. This is in contrast to (d) where also multiples of the frequencies $\pm A/2$ appear.

V. NONSINUSOIDAL CARRIER WAVE FORMS

We discuss now the possibility and opportunities of nonsinusoidal carrier wave forms for the electron and nuclear spins. Here, we focus on the nuclear spin as the maximal amplitude $v_{\max}$ limits the minimum polarization transfer times in the rotating frame. But similar arguments might also be used for the microwave carrier wave form in applications where the minimum duration of an experiment is limited by $u_{\max}$. As explained in Sec. II, we have considered so far a sinusoidal carrier wave form $\tilde{v}_x(t) = v(t)\cos[\omega_I^{\rm rf} t + \phi(t)]$, which is motivated by the limited bandwidth of typical radio-frequency wave form generators and amplifiers. Equation (11) determines the time-optimal radio-frequency Hamiltonian for transferring polarization from the state S_z to I_x in the rotating frame. In the laboratory frame, the corresponding radio-frequency Hamiltonian is given by

$$H^{\rm rf} = 4\pi v_{\max} \cos\left(\omega_I^{\rm rf} t - \pi/2\right) \mathrm{sgn}[\sin(\pi A t)]\, I_x. \qquad (16)$$

However, it is conceivable (e.g., for applications at low magnetic fields or for nuclei with small gyromagnetic ratios) that the resonance frequency and the corresponding carrier frequency $\omega_I^{\rm rf}$ of the controls are sufficiently small such that nonsinusoidal wave forms (containing higher harmonics of the carrier frequency $\omega_I^{\rm rf}$) can be created and amplified. One can therefore envision a radio-frequency Hamiltonian for the ideal case of infinite bandwidth as given by

$$\tilde{H}^{\rm rf} = 4\pi v_{\max}\, \mathrm{sgn}\big[\cos\left(\omega_I^{\rm rf} t - \pi/2\right)\big] \mathrm{sgn}[\sin(\pi A t)] I_x. \qquad (17)$$

Assuming the same maximal radio-frequency $2v_{\max}$ (in the laboratory frame) and switching from the Hamiltonian $H^{\rm rf}$ in Eq. (16) to the Hamiltonian $\tilde{H}^{\rm rf}$ in Eq. (17), the radio-frequency amplitude of the carrier frequency is implicitly increased in the rotating frame by another factor of $4/\pi$ (similarly as in discussed in Sec. IV). Consequently, the polarization transfer from the state S_z to I_x would be achievable using only $(\pi/4)^2 \approx 61.7\%$ of the conventional transfer time.

VI. CONCLUSION

We have presented time-optimal polarization transfers from an electron spin to a nuclear spin for the case of secular hyperfine couplings. In particular, we have analyzed the transfers from the electron-spin state S_z to the nuclear-spin states I_z and I_x. For the transfer to I_x, we could improve on the duration of on-resonance sinusoidal solutions by applying a control which has the form of a square wave. Our results also highlight differences between optimizations for minimum energy and minimum time. We have also discussed how these differences are related to bandwidth limitations.

On a more general scale, we have identified an important class of faster controls which appears under certain model assumptions (see Secs. III and IV A). Our proofs of the time optimality for the considered polarization transfers rely on the corresponding time-optimal implementations for all unitaries which achieve the transfer (see Secs. II and III). The analysis utilizes the specific structure and assumptions for the quantum system consisting of one electron spin and one nuclear spin [110], which imply that the control system has the form of a symmetric space [128]. This considerably simplifies our arguments [59,66], but other arguments are possible in certain cases (cf. [75–77,83,91]). Nevertheless, our technique for relating time-optimal implementations of polarization transfers and unitary propagators by determining all relevant unitary propagators (see Appendix A) illuminates how to apply it more generally, and it complements approaches featuring usually difficult to obtain maximal possible transfer amplitudes as a function of the control duration [59,64,65]. In particular, the provided analytic arguments employ the surjectivity of particular decompositions of unitaries into canonical coordinates (see Appendices A and B). All these techniques will be useful for analyzing the control structure of general quantum systems.

We close by briefly discussing how experimental constraints and imperfections can impact the proposed control schemes, which have been designed so that they take into account the maximal available control amplitude and the maximal bandwidth of the electronic system as determined by arbitrary wave form generators, amplifiers, and resonators. In Sec. IV A, we have also discussed how our analysis relates to control schemes with minimal total energy, but we have not considered experimental considerations about minimizing the total energy or average power usage more generally [129]. In addition to experimental constraints relating to the control amplitudes, experimental imperfections of the suggested control sequences might have to be considered in practical applications [130]. Potential experimental imperfections include unknown scaling factors of the control amplitudes due to the spatial inhomogeneity of the control field (i.e., the microwave and radio-frequency fields in the case of conventional DNP experiments using large ensembles of spin systems in macroscopic sample volumes [131,132]) or due to the experimental accuracy with which the control fields can be calibrated (e.g., in the case of individual spin systems in quantum information processing [14–17]). In addition, experimental imperfections are imperfectly calibrated pulse phases [133], amplitude and phase transients [106,134], timing errors in the creation and switching of of control amplitudes [133], slow temporal variations of control amplitudes (such as the so-called power droop due to heating effects in the electronics) [133], noise (i.e., fast temporal variations) on the control amplitudes based on imperfect electronics [135], and variations of the external magnetic field B_0. In particular, all these experimental imperfections will in general be of different size for the electron and nuclear control channels. For spectroscopic DNP applications, where fidelities above 0.98 would be more than sufficient, it is expected that currently available hardware and arbitrary wave form generators [106,136,137] should make it possible to realize the control schemes proposed here. In the case of quantum information applications with desired fidelities above 0.9999 more sophisticated corrections schemes might be required (e.g., pulse fixing [138]).

ACKNOWLEDGMENTS

H.Y. acknowledges the financial support from the Research Grants Council (RGC) of Hong Kong (Grant No. 538213). R.Z. and S.J.G. acknowledge support from the Deutsche Forschungsgemeinschaft (DFG) through Grant No. GL 203/7-1 and No. GL 203/7-2.

APPENDIX A: DECOMPOSITION OF UNITARIES

1. Unitaries which transfer $2S_zI_z$ to I_z

All unitaries in SU(4) can be be decomposed as K_1AK_2 with a slow evolution $A := \exp[-i(\alpha S^\alpha I_y + \beta S^\beta I_y)]$ and fast unitaries K_1 and K_2 which can be generated by controls on the electron spin and the secular hyperfine coupling (cf. [59,66,110,128]); recall that $S^\alpha = \left(\begin{smallmatrix}1 & 0\\ 0 & 0\end{smallmatrix}\right) \otimes \sigma_0$ and $S^\beta = \left(\begin{smallmatrix}0 & 0\\ 0 & 1\end{smallmatrix}\right) \otimes \sigma_0$. The unitaries that transfer $2S_zI_z$ to I_z can be determined as solutions to the matrix equation $I_z = K_1AK_2(2S_zI_z)K_2^\dagger A^\dagger K_1^\dagger$. The fast unitaries K_1 and K_2 can be parametrized using canonical coordinates of the second kind (see Sec. 2.8 of [139], Sec. 2.10 of [140], or Chap. III, Sec. 4.3 of [141]), i.e.,

$$K_1 := e^{-ia_7S_x}e^{-ia_6S_y}e^{-ia_5S_z} \times e^{-ia_42S_xI_z}e^{-ia_32S_yI_z}e^{-ia_22S_zI_z}e^{-ia_1I_z}, \quad \text{(A1a)}$$

$$K_2 := e^{-ib_1S_x}e^{-ib_2S_y}e^{-ib_32S_xI_z}e^{-ib_42S_yI_z} \times e^{-ib_5S_z}e^{-ib_62S_zI_z}e^{-ib_7I_z}. \quad \text{(A1b)}$$

The surjectivity of the representations in Eqs. (A1) is verified in Appendix B. As the unitary K_1 commutes with I_z and parts of K_2 commute with $2S_zI_z$, the matrix equation simplifies to

$$I_z = Ae^{-ib_1S_x}e^{-ib_2S_y}e^{-ib_32S_xI_z}e^{-ib_42S_yI_z}(2S_zI_z) \times e^{ib_42S_yI_z}e^{ib_32S_xI_z}e^{ib_2S_y}e^{ib_1S_x}A^\dagger.$$

With the help of the computer algebra system MAPLE [142], one can verify that either $\alpha = 2\pi z_1$ and $\beta = \pi + 2\pi z_2$ or $\alpha = \pi + 2\pi z_1$ and $\beta = 2\pi z_2$ with $z_1, z_2 \in \mathbb{Z}$ holds. In Sec. II of the main text, we focused on the first case assuming that $\alpha = 0$ and $\beta = \pi$ (i.e., $z_1 = z_2 = 0$); all other cases are similar.

2. Unitaries which transfer $2S_zI_z$ to I_x

Similarly as in Appendix A 1, the unitaries can be decomposed into a product K_1AK_2 of fast unitaries K_1, K_2, and a slow evolution $A = \exp[-i(\alpha S^\alpha I_y + \beta S^\beta I_y)]$. In particular, all unitaries which transfer $2S_zI_z$ to I_x have to satisfy the matrix equation $I_x = K_1AK_2(2S_zI_z)K_2^\dagger A^\dagger K_1^\dagger$. By observing trivial commutators, the matrix equation simplifies to

$$I_x = e^{-ia_42S_xI_z}e^{-ia_32S_yI_z}e^{-ia_22S_zI_z}e^{-ia_1I_z}A \times e^{-ib_1S_x}e^{-ib_2S_y}e^{-ib_32S_xI_z}e^{-ib_42S_yI_z}(2S_zI_z) \times e^{ib_42S_yI_z}e^{ib_32S_xI_z}e^{ib_2S_y}e^{ib_1S_x}A^\dagger \times e^{ia_1I_z}e^{ia_22S_zI_z}e^{ia_32S_yI_z}e^{ia_42S_xI_z}.$$

With the help of the computer algebra system MAPLE [142], one can infer that $\beta = \alpha - \pi + 2\pi z$ holds for $z \in \mathbb{Z}$. In Sec. III of the main text, we consider the case of $A = \exp[-\pi i S_z I_y]$ which corresponds to $\alpha = \pi/2$, $\beta = -\pi/2$, and $z = 0$. This choice is actually optimal: It follows from Eq. (6) in the main text that

$$\alpha = \int_0^T -2\pi [v_x(t)\sin(\pi At) - v_y(t)\cos(\pi At)]\,dt,$$

$$\beta = \int_0^T 2\pi [v_x(t)\sin(\pi At) + v_y(t)\cos(\pi At)]\,dt$$

holds for any given time T. Consequently, $\beta - \alpha = \int_0^T 4\pi v_x(t)\sin(\pi At)dt$. One applies the condition $\beta = \alpha - \pi + 2\pi z$ and obtains $\int_0^T 4\pi v_x(t)\sin(\pi At)dt = -\pi + 2\pi z$. This implies that

$$\left|\int_0^T 4\pi v_x(t)\sin(\pi At)dt\right| \geqslant |-\pi + 2\pi z| \geqslant \pi.$$

On the other hand, one has $|\int_0^T 4\pi v_x(t)\sin(\pi At)dt| \leqslant \int_0^T 4\pi v_{\max}|\sin(\pi At)|dt = 8v_{\max}T$ (see Sec. III). In order to satisfy the condition $\beta = \alpha - \pi + 2\pi z$, the time T has to fulfill the inequality $8v_{\max}T \geqslant \pi$. One gets a lower bound $T_{\min} \geqslant \pi/(8v_{\max})$ on the minimum time $T_{\min}$. In summary, the scheme presented in Sec. III of the main text is optimal as it saturates the lower bound.

APPENDIX B: VERIFICATION OF THE SURJECTIVITY OF THE REPRESENTATIONS IN EQ. (A1)

In order to verify the surjectivity of K_1 in Eq. (A1a) it is sufficient to verify the surjectivity of the product

$$\begin{aligned}\tilde{K}_1 &= \tilde{K}_1(a_7,a_6,a_5,a_4,a_3,a_2)\\ &:= e^{-ia_7S_x}e^{-ia_6S_y}e^{-ia_5S_z}e^{-ia_4 2S_xI_z}e^{-ia_3 2S_yI_z}e^{-ia_2 2S_zI_z}\end{aligned}$$

which consists of the first six elements of K_1 as the seventh element commutes with all the other ones. First we show that there exists a_4', a_3', and a_2' such that

$$\begin{aligned}&e^{-ia_7S_x}e^{-ia_6S_y}e^{-ia_5S_z}e^{-ia_4 2S_xI_z}e^{-ia_3 2S_yI_z}e^{-ia_2 2S_zI_z}\\ &\quad= e^{-ia_4' 2S_xI_z}e^{-ia_3' 2S_yI_z}e^{-ia_2' 2S_zI_z}e^{-ia_7S_x}e^{-ia_6S_y}e^{-ia_5S_z},\end{aligned} \tag{B1}$$

which can be written as

$$\begin{aligned}&e^{-ia_4' 2S_xI_z}e^{-ia_3' 2S_yI_z}e^{-ia_2' 2S_zI_z}\\ &\quad= e^{-ia_7S_x}e^{-ia_6S_y}e^{-ia_5S_z}(e^{-ia_4 2S_xI_z}e^{-ia_3 2S_yI_z}e^{-ia_2 2S_zI_z})\\ &\qquad\times e^{ia_5S_z}e^{ia_6S_y}e^{ia_7S_x}.\end{aligned}$$

The effect of the conjugation with $\exp(-ia_5S_z)$ is

$$\begin{aligned}&e^{-ia_5S_z}e^{-ia_4 2S_xI_z}e^{-ia_3 2S_yI_z}e^{-ia_2 2S_zI_z}e^{ia_5S_z}\\ &\quad= e^{-ia_5S_z}e^{-ia_4 2S_xI_z}e^{ia_5S_z}\\ &\qquad\times e^{-ia_5S_z}e^{-ia_3 2S_yI_z}e^{ia_5S_z}e^{-ia_5S_z}e^{-ia_2 2S_zI_z}e^{ia_5S_z}\\ &\quad= e^{-ia_4[\cos(a_5)2S_xI_z+\sin(a_5)2S_yI_z]}\\ &\qquad\times e^{-ia_3[\cos(a_5)2S_yI_z-\sin(a_5)2S_xI_z]}e^{-ia_2 2S_zI_z}\\ &\quad= e^{-ia_4''2S_xI_z}e^{-ia_3''2S_yI_z}e^{-ia_2''2S_zI_z},\end{aligned}$$

where the last step follows from the Euler-angle decomposition. Similar arguments for the conjugations with $e^{-ia_6S_y}$ and $e^{-ia_7S_x}$ demonstrate Eq. (B1). Any element in the connected Lie group that is infinitesimally generated by the elements $-iS_x$, $-iS_y$, $-iS_z$, $-i2S_xI_z$, $-i2S_yI_z$, and $-i2S_zI_z$ can be achieved by a finite product of elements having the form of $\tilde{K}_1$; this is a consequence of Lemma 6.2 in [143]. We apply Eq. (B1) and the Euler-angle decomposition multiple times and obtain $\tilde{K}_1(a_7,a_6,a_5,a_4,a_3,a_2)\tilde{K}_1(\tilde{a}_7,\tilde{a}_6,\tilde{a}_5,\tilde{a}_4,\tilde{a}_3,\tilde{a}_2) = \tilde{K}_1(c_7,c_6,c_5,c_4,c_3,c_2)$ for certain values of c_7, c_6, c_5, c_4, c_3, and c_2. In summary, we have verified the surjectivity of the representations $\tilde{K}_1$ and K_1.

Similar as for Eq. (B1), one can verify that

$$e^{-ia_5S_z}e^{-ia_4 2S_xI_z}e^{-ia_3 2S_yI_z} = e^{-ia_4' 2S_xI_z}e^{-ia_3' 2S_yI_z}e^{-ia_5S_z}$$

holds for some a_4' and a_3'. Consequently, the surjectivity of K_1 implies the surjectivity of K_2.

An alternative second argument for the surjectivity of Eq. (A1a) applies the decomposition $K_1'A'K_2'$ for the set $K = \exp(\mathfrak{k})$ of all fast operations where $K_i' = \exp(\mathfrak{k}')$ and $A' = \exp(\mathfrak{a}')$. This decomposition is a consequence of the Cartan decomposition $\mathfrak{k} = \mathfrak{k}' \oplus \mathfrak{p}'$ where the corresponding linear subspaces are given by $\mathfrak{k}' := \mathrm{span}\{-iS_x,-iS_y,-iS_z,-iI_z\}$, $\mathfrak{p}' := \mathrm{span}\{-i2S_xI_z,-i2S_yI_z,-i2S_zI_z\}$, and the Abelian subalgebra $\mathfrak{a}' := \mathrm{span}\{-i2S_zI_z\} \subseteq \mathfrak{p}'$ [128]. The decomposition $K_1'A'K_2'$ implies that the decomposition

$$\begin{aligned}U' = Ue^{i\pi S_zI_z} &= e^{-id_1S_x}e^{-id_2S_y}e^{-id_3S_z}e^{-id_4 2S_zI_z}\\ &\quad\times e^{-id_5S_z}e^{-id_6S_x}e^{-id_7S_y}e^{-id_8I_z}\end{aligned}$$

is a surjective parametrization of the set of all fast operations. Therefore, the surjectivity is also verified for

$$\begin{aligned}U &= e^{-id_1S_x}e^{-id_2S_y}e^{-id_3S_z}e^{-id_4 2S_zI_z}\\ &\quad\times e^{-id_5S_z}e^{-id_6S_x}e^{-id_7S_y}e^{-id_8I_z}e^{-i\pi S_zI_z}\\ &= e^{-id_1S_x}e^{-id_2S_y}e^{-i(d_3+d_5)S_z}e^{-i(d_4+\pi/2)2S_zI_z}\\ &\quad\times e^{id_6 2S_yI_z}e^{-id_7 2S_xI_z}e^{-id_8I_z}\\ &= e^{-id_1S_x}e^{-id_2S_y}e^{-id_3'S_z}e^{-id_4' 2S_xI_z}\\ &\quad\times e^{-id_5' 2S_yI_z}e^{-id_5' 2S_zI_z}e^{-id_8I_z},\end{aligned}$$

where the last equality follows from the Euler-angle decomposition. This completes the second argument for the surjectivity of Eq. (A1a).

[1] A. Schweiger and G. Jeschke, *Principles of Pulse Electron Parametric Resonance* (Oxford University Press, Oxford, 2010).

[2] H. Brunner, R. H. Fritsch, and K. H. Hausser, Z. Naturforsch. A **42**, 1456 (1987).

[3] V. Weis and R. G. Griffin, Solid State Nucl. Magn. Reson. **29**, 66 (2006).

[4] G. W. Morley, J. van Tol, A. Ardavan, K. Porfyrakis, J. Zhang, and G. A. Briggs, Phys. Rev. Lett. **98**, 220501 (2007).

[5] T. Maly, G. T. Debelouchina, V. S. Bajaj, K.-N. Hu, C.-G. Joo, M.-L. Mak-Jurkauskas, J. R. Sirigiri, P. C. A. van der Wel, J. Herzfeld, R. J. Temkin, and R. G. Griffin, J. Chem. Phys. **128**, 052211 (2008).

[6] C. Griesinger, M. Bennati, H. M. Vieth, C. Luchinat, G. Parigi, P. Höfer, F. Engelke, S. J. Glaser, V. Denysenkov, and T. F. Prisner, Prog. Nucl. Magn. Reson. Spectrosc. **64**, 4 (2012).

[7] M. H. Levitt, *Spin Dynamics: Basics of Nuclear Magnetic Resonance* (Wiley, New York, 2008).

[8] R. R. Ernst, G. Bodenhausen, and A. Wokaun, *Principles of Nuclear Magnetic Resonance in One and Two Dimensions* (Clarendon, Oxford, 1987).

[9] M. Mehring, J. Mende, and W. Scherer, Phys. Rev. Lett. **90**, 153001 (2003).

[10] W. Scherer and M. Mehring, J. Chem. Phys. **128**, 052305 (2008).

[11] B. Naydenov, J. Mende, W. Harneit, and M. Mehring, Phys. Status Solidi B **245**, 2002 (2008).

[12] J. J. L. Morton, A. M. Tyryshkin, A. Ardavan, K. Porfyrakis, S. A. Lyon, and G. A. D. Briggs, Phys. Rev. B **76**, 085418 (2007).

[13] J. J. L. Morton, A. M. Tyryshkin, R. M. Brown, S. Shankar, B. W. Lovett, A. Ardavan, T. Schenkel, E. E. Haller, J. W. Ager, and S. A. Lyon, Nature (London) **455**, 1085 (2008).

[14] F. Jelezko, T. Gaebel, I. Popa, M. Domhan, A. Gruber, and J. Wrachtrup, Phys. Rev. Lett. **93**, 130501 (2004).

[15] L. Childress, M. V. Gurudev Dutt, J. M. Taylor, A. S. Zibrov, F. Jelezko, J. Wachtrup, P. R. Hemmer, and M. D. Lukin, Science **314**, 281 (2006).

[16] G. Waldherr, Y. Wang, S. Zaiser, M. Jamali, T. Schulte-Herbrüggen, H. Abe, T. Ohshima, J. Isoya, J. F. Du, P. Neumann, and J. Wrachtrup, Nature (London) **506**, 204 (2014).

[17] C. Müller, X. Kong, J.-M. Cai, K. Melentijević, A. Stacey, M. Markham, D. Twitchen, J. Isoya, S. Pezzagna, J. Meijer, J. F. Du, M. B. Plenio, B. Naydenov, L. P. McGuinness, and F. Jelezko, Nat. Commun. **5**, 4703 (2014).

[18] W. S. Warren, H. Rabitz, and M. Dahlen, Science **259**, 1581 (1993).

[19] S. Rice and M. Zhao, *Optimal Control of Quantum Dynamics* (Wiley, New York, 2000).

[20] M. Shapiro and P. Brumer, *Principles of Quantum Control of Molecular Processes* (Wiley, New York, 2003).

[21] D. J. Tannor, *Introduction to Quantum Mechanics: A Time-Dependent Perspective* (University Science Books, Sausalito, 2007).

[22] D. D'Alessandro, *Introduction to Quantum Control and Dynamics* (Chapman & Hall/CRC, Boca Raton, 2008).

[23] C. Brif, R. Chakrabarti, and H. Rabitz, New J. Phys. **12**, 075008 (2010).

[24] A. E. Bryson and Y.-C. Ho, *Applied Optimal Control: Optimization, Estimation, and Control* (Hemisphere Publishing, Washington, DC, 1975).

[25] S. Conolly, D. Nishimura, and A. Macovski, IEEE Trans. Med. Imaging **5**, 106 (1986).

[26] A. P. Peirce, M. A. Dahleh, and H. Rabitz, Phys. Rev. A **37**, 4950 (1988).

[27] S. Shi, A. Woody, and H. Rabitz, J. Chem. Phys. **88**, 6870 (1988).

[28] V. F. Krotov, *Global Methods in Optimal Control* (Marcel Dekker, New York, 1996).

[29] Y. Ohtsuki, W. Zhu, and H. Rabitz, J. Chem. Phys. **110**, 9825 (1999).

[30] A. I. Konnov and V. F. Krotov, Autom. Remote Control **60**, 1427 (1999), Russian orig.: Avtom. Telemekh. **1999**, 77 (1999).

[31] J. P. Palao and R. Kosloff, Phys. Rev. A **68**, 062308 (2003).

[32] Y. Ohtsuki, G. Turinici, and H. Rabitz, J. Chem. Phys. **120**, 5509 (2004).

[33] N. Khaneja, T. Reiss, C. Kehlet, T. Schulte-Herbrüggen, and S. J. Glaser, J. Magn. Reson. **172**, 296 (2005).

[34] Z. Tošner, T. Vosegaard, C. T. Kehlet, N. Khaneja, S. J. Glaser, and N. C. Nielsen, J. Magn. Reson. **197**, 120 (2009).

[35] S. Machnes, U. Sander, S. J. Glaser, P. de Fouquières, A. Gruslys, S. Schirmer, and T. Schulte-Herbrüggen, Phys. Rev. A **84**, 022305 (2011).

[36] P. de Fouquieres, S. G. Schirmer, S. J. Glaser, and I. Kuprov, J. Magn. Reson. **212**, 412 (2011).

[37] R. Eitan, M. Mundt, and D. J. Tannor, Phys. Rev. A **83**, 053426 (2011).

[38] L. S. Pontryagin, V. G. Boltyanskii, R. V. Gamkrelidze, and E. F. Mishchenko, *The Mathematical Theory of Optimal Processes* (Wiley, New York, 1962).

[39] V. Jurdjevic, *Geometric Control Theory* (Cambridge University Press, Cambridge, 1997).

[40] B. Bonnard and M. Chyba, *Singular Trajectories and Their Role in Control Theory*, Mathématiques et Applications Vol. 40 (Springer, Berlin, 2003).

[41] U. Boscain and B. Piccoli, *Optimal Syntheses for Control on 2-D Manifolds*, Mathématiques et Applications Vol. 43 (Springer, Berlin, 2004).

[42] D. J. Tannor and A. Bartana, J. Phys. Chem. A **103**, 10359 (1999).

[43] U. Boscain, G. Charlot, J.-P. Gauthier, and H.-R. Jauslin, J. Math. Phys. **43**, 2107 (2002).

[44] U. Boscain, T. Chambrion, and G. Charlot, Discrete Contin. Dyn. Syst. Ser. B **5**, 957 (2005).

[45] U. Boscain and P. Mason, J. Math. Phys. **47**, 062101 (2006).

[46] D. Sugny, C. Kontz, and H. R. Jauslin, Phys. Rev. A **76**, 023419 (2007).

[47] B. Bonnard and D. Sugny, SIAM J. Control Optim. **48**, 1289 (2009).

[48] B. Bonnard, M. Chyba, and D. Sugny, IEEE Trans. Autom. Control **54**, 2598 (2009).

[49] M. Lapert, Y. Zhang, M. Braun, S. J. Glaser, and D. Sugny, Phys. Rev. Lett. **104**, 083001 (2010).

[50] M. Lapert, Y. Zhang, S. J. Glaser, and D. Sugny, J. Phys. B **44**, 154014 (2011).

[51] Y. Zhang, M. Lapert, D. Sugny, M. Braun, and S. J. Glaser, J. Chem. Phys. **134**, 054103 (2011).

[52] A. D. Boozer, Phys. Rev. A **85**, 012317 (2012).

[53] V. Mukherjee, A. Carlini, A. Mari, T. Caneva, S. Montangero, T. Calarco, R. Fazio, and V. Giovannetti, Phys. Rev. A **88**, 062326 (2013).

[54] A. Garon, S. J. Glaser, and D. Sugny, Phys. Rev. A **88**, 043422 (2013).

[55] M. Lapert, E. Assémat, S. J. Glaser, and D. Sugny, Phys. Rev. A **88**, 033407 (2013).

[56] F. Albertini and D. D'Alessandro, J. Math. Phys. **56**, 012106 (2015).

[57] E. Assémat, M. Lapert, Y. Zhang, M. Braun, S. J. Glaser, and D. Sugny, Phys. Rev. A **82**, 013415 (2010).

[58] E. Assémat, L. Attar, M.-J. Penouilh, M. Picquet, A. Tabard, Y. Zhang, S. J. Glaser, and D. Sugny, Chem. Phys. **405**, 71 (2012).

[59] N. Khaneja, R. Brockett, and S. J. Glaser, Phys. Rev. A **63**, 032308 (2001).

[60] C. H. Bennett, J. I. Cirac, M. S. Leifer, D. W. Leung, N. Linden, S. Popescu, and G. Vidal, Phys. Rev. A **66**, 012305 (2002).

[61] G. Vidal, K. Hammerer, and J. I. Cirac, Phys. Rev. Lett. **88**, 237902 (2002).

[62] K. Hammerer, G. Vidal, and J. I. Cirac, Phys. Rev. A **66**, 062321 (2002).

[63] H. Yuan and N. Khaneja, Phys. Rev. A **72**, 040301(R) (2005).

[64] T. O. Reiss, N. Khaneja, and S. J. Glaser, J. Magn. Reson. **154**, 192 (2002).

[65] N. Khaneja, F. Kramer, and S. J. Glaser, J. Magn. Reson. **173**, 116 (2005).

[66] N. Khaneja, S. J. Glaser, and R. Brockett, Phys. Rev. A **65**, 032301 (2002).

[67] N. Khaneja and S. J. Glaser, Phys. Rev. A **66**, 060301(R) (2002).

[68] T. O. Reiss, N. Khaneja, and S. J. Glaser, J. Magn. Reson. **165**, 95 (2003).

[69] S. Bose, Phys. Rev. Lett. **91**, 207901 (2003).

[70] R. Zeier, M. Grassl, and T. Beth, Phys. Rev. A **70**, 032319 (2004).

[71] D. Stefanatos, N. Khaneja, and S. J. Glaser, Phys. Rev. A **69**, 022319 (2004).

[72] D. Stefanatos, S. J. Glaser, and N. Khaneja, Phys. Rev. A **72**, 062320 (2005).

[73] T. Schulte-Herbrüggen, A. K. Spörl, N. Khaneja, and S. J. Glaser, Phys. Rev. A **72**, 042331 (2005).

[74] A. Carlini, A. Hosoya, T. Koike, and Y. Okudaira, Phys. Rev. Lett. **96**, 060503 (2006).

[75] N. Khaneja, B. Heitmann, A. Spörl, H. Yuan, T. Schulte-Herbrüggen, and S. J. Glaser, Phys. Rev. A **75**, 012322 (2007).

[76] H. Yuan, S. J. Glaser, and N. Khaneja, Phys. Rev. A **76**, 012316 (2007).

[77] H. Yuan, R. Zeier, and N. Khaneja, Phys. Rev. A **77**, 032340 (2008).

[78] S. G. Schirmer and P. J. Pemberton-Ross, Phys. Rev. A **80**, 030301 (2009).

[79] D. Burgarth, K. Maruyama, M. Murphy, S. Montangero, T. Calarco, F. Nori, and M. B. Plenio, Phys. Rev. A **81**, 040303 (2010).

[80] X. Wang, A. Bayat, S. Bose, and S. G. Schirmer, Phys. Rev. A **82**, 012330 (2010).

[81] X. Wang, A. Bayat, S. G. Schirmer, and S. Bose, Phys. Rev. A **81**, 032312 (2010).

[82] A. Carlini, A. Hosoya, T. Koike, and Y. Okudaira, J. Phys. A **44**, 145302 (2011).

[83] H. Yuan and N. Khaneja, Phys. Rev. A **84**, 062301 (2011).

[84] M. Lapert, J. Salomon, and D. Sugny, Phys. Rev. A **85**, 033406 (2012).

[85] A. Carlini and T. Koike, Phys. Rev. A **86**, 054302 (2012).

[86] M. Nimbalkar, R. Zeier, J. L. Neves, S. B. Elavarasi, H. Yuan, N. Khaneja, K. Dorai, and S. J. Glaser, Phys. Rev. A **85**, 012325 (2012).

[87] A. Carlini and T. Koike, J. Phys. A **46**, 045307 (2013).

[88] B. Bonnard, O. Cots, and N. Shcherbakova, Math. Control Related Fields **3**, 287 (2013).

[89] B. Bonnard, O. Cots, J.-B. Pomet, and N. Shcherbakova, ESAIM Control Optim. Calc. Var. **20**, 864 (2014).

[90] H. Yuan, D. Wei, Y. Zhang, S. Glaser, and N. Khaneja, Phys. Rev. A **89**, 042315 (2014).

[91] L. Van Damme, R. Zeier, S. J. Glaser, and D. Sugny, Phys. Rev. A **90**, 013409 (2014).

[92] E. M. Fortunato, M. A. Pravia, N. Boulant, G. Teklemariam, T. F. Havel, and D. G. Cory, J. Chem. Phys. **116**, 7599 (2002).

[93] N. C. Nielsen, C. Kehlet, S. J. Glaser, and N. Khaneja, Encycl. Nucl. Magn. Reson. **9**, 100 (2010).

[94] T. E. Skinner, T. O. Reiss, B. Luy, N. Khaneja, and S. J. Glaser, J. Magn. Reson. **163**, 8 (2003).

[95] T. E. Skinner, T. O. Reiss, B. Luy, N. Khaneja, and S. J. Glaser, J. Magn. Reson. **167**, 68 (2004).

[96] K. Kobzar, T. E. Skinner, N. Khaneja, S. J. Glaser, and B. Luy, J. Magn. Reson. **170**, 236 (2004).

[97] L. P. Pryadko and P. Sengupta, Phys. Rev. A **78**, 032336 (2008).

[98] J. L. Neves, B. Heitmann, N. Khaneja, and S. J. Glaser, J. Magn. Reson. **201**, 7 (2009).

[99] F. Schilling and S. J. Glaser, J. Magn. Reson. **223**, 207 (2012).

[100] F. Zhang, F. Schilling, S. J. Glaser, and C. Hilty, Anal. Chem. **85**, 2875 (2013).

[101] V. D. M. Koroleva, S. Mandal, Y.-Q. Song, and M. D. Hürlimann, J. Magn. Reson. **230**, 64 (2013).

[102] F. Schilling, N. I. Warner, T. E. Gershenzon, M. Sattler, and S. J. Glaser, Angew. Chem., Int. Ed. **53**, 4475 (2014).

[103] W. A. Grissom, D. Xu, A. B. Kerr, and J. A. Fessler, IEEE Trans. Med. Imag. **28**, 1548 (2009).

[104] H. Liu and G. B. Matson, Magn. Reson. Med. **66**, 1254 (2011).

[105] M. Lapert, Y. Zhang, M. A. Janich, S. J. Glaser, and D. Sugny, Sci. Rep. **2**, 589 (2012).

[106] P. E. Spindler, Y. Zhang, B. Endeward, N. Gershernzon, T. E. Skinner, S. J. Glaser, and T. Prisner, J. Magn. Reson. **218**, 49 (2012).

[107] N. Khaneja, Phys. Rev. A **76**, 032326 (2007).

[108] J. S. Hodges, J. C. Yang, C. Ramanathan, and D. G. Cory, Phys. Rev. A **78**, 010303 (2008).

[109] I. I. Maximov, Z. Tošner, and N. C. Nielsen, J. Chem. Phys. **128**, 184505 (2008).

[110] R. Zeier, H. Yuan, and N. Khaneja, Phys. Rev. A **77**, 032332 (2008).

[111] N. Pomplun, B. Heitmann, N. Khaneja, and S. J. Glaser, Appl. Magn. Reson. **34**, 331 (2008).

[112] N. Pomplun, Ph.D. thesis, Technische Universität München, 2010.

[113] N. Pomplun and S. J. Glaser, Phys. Chem. Chem. Phys. **12**, 5791 (2010).

[114] Note that we only consider the (rescaled) traceless part ρ of the actual density matrix $b\rho + \frac{1}{4}I$, where b denotes the Boltzmann factor. As the identity component does not evolve, it can be neglected.

[115] In [110], the choice for ω_I^{off} was $\omega_I^{\text{off}} = \pi A$.

[116] Strictly speaking, our results are also applicable when only the conditions $A \gg v_{\max}$ and $u_{\max} \gg v_{\max}$ are fulfilled.

[117] The notation $A \xrightarrow{B} C$ describes that polarization is transferred from A to C by applying the unitary transfer $C = \exp(-iB)A\exp(iB)$.

[118] G. A. Morris and R. Freeman, J. Am. Chem. Soc. **101**, 760 (1979).
[119] J. Keeler, *Understanding NMR Spectroscopy*, 2nd ed. (Wiley, Chichester, UK, 2010).
[120] In the interaction frame, $H_{\rm rot}$ is transformed into $H_{\rm int} = \exp(i2\pi AS_zI_zt)H_{\rm rot}\exp(-i2\pi AS_zI_zt) - 2\pi AS_zI_z$.
[121] J. Feeney and P. Partington, J. Chem. Soc. Chem. Commun. **1973**, 611 (1973).
[122] K. G. R. Pachler and P. L. Wessels, J. Magn. Reson. **12**, 337 (1973).
[123] R. A. Craig, R. K. Harris, and R. J. Morrow, Org. Magn. Reson. **13**, 229 (1980).
[124] O. W. Sørensen, Prog. Nucl. Magn. Reson. Spectrosc. **21**, 503 (1989).
[125] Even though we have $u_{\max} < A$, the crucial requirements $A \gg v_{\max}$ and $u_{\max} \gg v_{\max}$ for optimality are fulfilled.
[126] R. L. Allen and D. W. Mills, *Signal Analysis* (IEEE, Piscataway, NJ, 2004).
[127] S. S. Köcher, T. Heydenreich, and S. J. Glaser, J. Magn. Reson. **249**, 63 (2014).
[128] S. Helgason, *Differential Geometry, Lie Groups, and Symmetric Spaces* (American Mathematical Society, Providence, 2001), reprinted with corrections.
[129] K. Kobzar, T. E. Skinner, N. Khaneja, S. J. Glaser, and B. Luy, J. Magn. Reson. **194**, 58 (2008).
[130] S. Glaser, U. Boscain, T. Calarco, C. Koch, W. Köckenberger, R. Kosloff, I. Kuprov, B. Luy, S. Schirmer, T. Schulte-Herbrüggen, D. Sugny, and F. Wilhelm, Eur. Phys. J. D (to be published), see also arXiv:1508.00442.
[131] T. E. Skinner, K. Kobzar, B. Luy, R. Bendall, W. Bermel, N. Khaneja, and S. J. Glaser, J. Magn. Reson. **179**, 241 (2006).
[132] T. E. Skinner, M. Braun, K. Woelk, N. I. Gershenzon, and S. J. Glaser, J. Magn. Reson. **209**, 282 (2011).
[133] R. Prigl and U. Haeberlen, in *Advances in Magnetic and Optical Resonance*, edited by W. S. Warren (Academic Press, San Diego, 1996), Vol. 19, pp. 1–58.
[134] I. N. Hincks, C. E. Granade, T. W. Borneman, and D. G. Cory, Phys. Rev. Appl. **4**, 024012 (2015).
[135] S. Kallush, M. Khasin, and R. Kosloff, New J. Phys. **16**, 015008 (2014).
[136] T. Kaufmann, T. J. Keller, J. M. Franck, R. P. Barnes, S. J. Glaser, J. M. Martinis, and S. Han, J. Magn. Reson. **235**, 95 (2013).
[137] A. Doll, S. Pribitzer, R. Tschaggelar, and G. Jeschke, J. Magn. Reson. **230**, 27 (2013).
[138] D. Lu, A. Brodurch, J. Park, H. Katiyar, and R. Jochym-O'Conner, T. Laflamme, arXiv:1501.01353.
[139] D. Elliott, *Bilinear Control Systems: Matrices in Action* (Springer, London, 2009).
[140] V. S. Varadarajan, *Lie Groups, Lie Algebras, and Their Representations* (Springer, New York, 1984).
[141] N. Bourbaki, *Lie Groups and Lie Algebras: Chapters 1–3* (Springer, Berlin, 1989).
[142] Maplesoft, Maple 18 (2014).
[143] V. Jurdjevic and H. Sussmann, J. Diff. Eq. **12**, 313 (1972).